Nonempirical Statistical Theory for Atomic Evaporation from Nonrigid Clusters: Applications to the Absolute Rate Constant and Kinetic Energy Release

Mikiya Fujii* and Kazuo Takatsuka†

Department of Basic Science, Graduate School of Arts and Sciences, University of Tokyo, Komaba, 153-8902 Tokyo, Japan

Received: October 30, 2006; In Final Form: December 18, 2006

A high energy atomic cluster undergoing frequent structural isomerization behaves like a liquid droplet, from which atoms or molecules can be emitted. Even after evaporation, the daughter cluster may still keep changing its structure. We study the dynamics of such an evaporation process of atomic evaporation. To do so, we develop a statistical rate theory for dissociation of highly nonrigid molecules and propose a simple method to calculate the *absolute value* of classical phase-space volume for a potential function that has many locally stable basins. The statistical prediction of the final distribution of the released kinetic energy is also developed. A direct application of the Rice−Ramsperger−Kassed−Marcus (RRKM) theory to this kind of multichannel chemical reaction is prohibitively difficult, unless further modeling and/or assumptions are made. We carry out a completely nonempirical statistical calculation for these dynamical quantities, in that nothing empirical is introduced like remodeling (or reparametrization) of artificial potential energy functions or recalibration of the phase-space volume referring to other "empirical" values such as those estimated with the molecular dynamics method. The so-called dividing surface is determined variationally, at which the flux is calculated in a consistent manner with the estimate of the phase-space volume in the initial state. Also, for the correct treatment of a highly nonrigid cluster, the phase-space volume and flux are estimated without the separation of vibrational and rotational motions. Both the microcanonical reaction rate and the final kinetic energy distribution thus obtained have quite accurately reproduced the corresponding quantities given by molecular dynamics calculations. This establishes the validity of the statistical arguments, which in turn brings about the deeper physical insight about the evaporation dynamics.

I. Introduction

Dynamics of clusters is very interesting and important in that it provides a characteristic opportunity to study the fundamental features, concepts, and laws of chemical reaction dynamics. In particular, the isomerization dynamics of atomic clusters and van der Waals clusters composed of identical atoms can be studied from the view points of, for instance, cooperative dynamics, the onset of statistical behavior (links between dynamics and statistical mechanics), and quantum effects including permutation symmetry in the mesoscopic scale. Argon clusters are among such objects that have been studied very intensively in the last two decades. All these features arise from a single fact that its potential function has many local minima to support locally stable molecular structures. Therefore, this isomerization dynamics is a typical example of the so-called many-valley (multiminimum) dynamics. Indeed, the isomerization dynamics of argon clusters has been studied in various aspects: microcanonical analog of the first-order solid−liquid phase transitions,[1−4] prototype of multichannel chemical reactions,[5−12] and kinematic effect of molecular internal space,[13−16] semiclassical quantization of chaos in isomerization dynamics.[17] They are sometimes studied with an emphasis on chaos and regularity in Hamiltonian many body systems[18−23] Also, the potential landscape for cluster dynamics have been explored extensively.[24−26]

In this paper we study the evaporation dynamics of an atomic Morse cluster, e.g., Ar_8, which undergoes dissociation reactions $Ar_8 \rightarrow Ar_7 + Ar$. [A molecular evaporation $Ar_8 \rightarrow Ar_6 + Ar_2$ will be reported elsewhere.[27]] As studied extensively in the literature cited above, Ar_8 undergoes frequent structural isomerization among eight locally stable isomers in an energy range that is lower than evaporation can take place (see Figure 1). (Likewise, Ar_7 has four isomers.) Therefore, it is quite interesting to see whether the structural transition may occur simultaneously in the course of dissociation. This is really the case as will be explicitly shown later with classical trajectory calculation. That is, isomerization and dissociation strongly couple with each other in comparable time scales, and hence, this evaporation dynamics is a typical example of multichannel dissociation reaction of highly nonrigid molecules. On the other hand, because of the high energy required by evaporation and the high anharmonicity of the potential energy surface, the reaction should be more or less stochastic. We are thus tempted to apply a statistical reaction theory such as the transition state theory or the RRKM theory for unimolecular dissociation.[28] However, it is immediately noticed that the present evaporation dynamics is not simple enough to allow their straightforward application for the following reasons: (1) There is not a transition state on the potential energy surface. (2) There are many reaction coordinates that strongly couple with each other. (3) Due to the frequent isomerization accompanying the dissociation, the molecule is highly nonrigid like a liquid droplet, which prohibits the separation of vibrational and rotational

* Corresponding author. E-mail: futofuji@mns2.c.u-tokyo.ac.jp.
† E-mail: kaztak@mns2.c.u-tokyo.ac.jp.

10.1021/jp067110y CCC: $37.00
Published on Web 02/06/2007

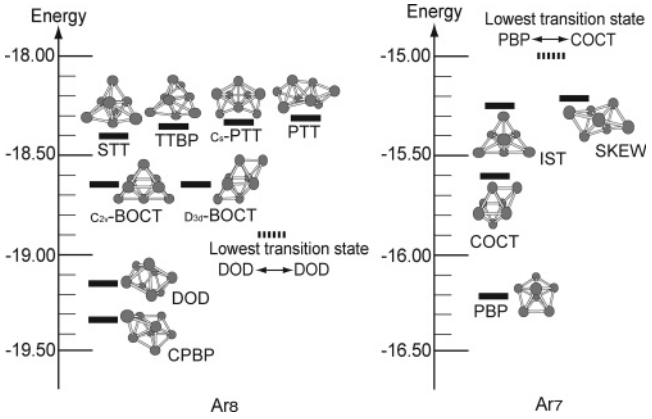

Figure 1. (left) Eight local minima of Ar_8. Their minimum energies are −19.327 for capped pentagonal bipyramid (CPBP), −19.162 for dodecadeltahedron (DOD), −18.645 for C_{2v}-bicapped octahedron (C_{2v}-BOCT), −18.641 for D_{3d}-bicapped octahedron (D_{3d}-BOCT), −18.404 for stellated tetrahedron (STT), −18.341 for tricapped trigonal bipyramid (TTBP), −18.323 for C_s-polytetrahedral (C_s-PTT), and −18.306 for polytetrahedral (PTT). (right) Four locally stable structures of Ar_7. The minimum energies are −16.208 for pentagonal bipyramid (PBP), −15.563 for capped octahedron (COCT), −15.248 for incomplete stellated tetrahedron (IST), and −15.216 for bicapped trigonal bipyramid (SKEW).

modes. (4) Under the nonseparability of vibration and rotation, both the phase-space volume and the flux at a dividing surface, which is a manifold dividing configurational space into reactant and product subspaces, are hard to calculate. These items constitute the central and most crucial task in the application of any statistical reaction theory. In this paper, we attempt to resolve these problems and thereby examine how statistical theory can work for this problem. In doing so, we actually resort to the original idea of phase-space theory.[29−31] (Because the work of Light[31] contains important generalization of the original phase-space theory (PST)[29] so as to calculate the product distribution under a constraint of symmetry, it is quite often that the Light theory is just referred to as phase-space theory. However, as phase-space theory the present paper refers back to the rather primitive concept of Wigner.)

There are two very important previous studies, among others, in the statistical study of evaporation dynamics of clusters. One is due to Amar and his co-workers,[32−34] and the other is by Calvo and his co-workers.[35−39] In particular, our work is an extension of phase-space theory of Calvo[35] so as to include the nonempirical calculations of the flux and the relevant phase-space volumes and the variational determination of the dividing surface. Their works are based on the fundamental paper of Chesnavich and Bower[40] about energy and angular momentum conservation incorporated into phase-space theory. (Incidentally, see refs 41 and 42 for an extensive discussion on the resolution of orbital angular momentum of relative motion of two dissociating molecules within the scheme of statistical reaction theory.) In phase-space theory, the relevant computation process is generally factored into two parts: one is the evaluation of the phase-space volume of a reactant, and the other is the flux at some critical place like the transition state. For the part of the phase-space volume, Weerasinghe and Amar[32] have applied the Nosé dynamics sampling with the multiple histogram method, and to determine the absolute magnitude of the density, they further applied the adiabatic switching method.[43,44] Similarly, Calvo et al. have used the sophisticated version of the Monte Carlo method,[35] but only the relative values of the phase-space volume were necessary for their studies. In calculating the flux, Chesnavich and Bower approximate a molecular system by a receding pair of rigid bodies like spherical top and linear top, and they take a rigorous account of angular momenta by assuming (or constructing) an empirical potential energy curve in the form r^{-p}, with r and p being, respectively, the mutual distance between the two tops and a parameter predetermined separately. This remodeling is particularly useful for an estimate of the rotational distribution of the products. Both Amar's and Calvo's groups have adopted this basic idea with individual adaptation to their own frameworks. Although this approximation must be good for a reaction having a tight transition state, its straightforward application to the dynamics of evaporation from a nonrigid cluster would not be appropriate, in which the coupling between vibration and rotation is strong. Besides, theoretical consistency between the evaluations of the flux at the dividing surface (or the transition state) and the phase-space volume of a reactant is lost as soon as the remodeled potential function is introduced. Even with these most advanced theoretical methods, it is still hard to carry out statistical calculations in a systematic and nonempirical manner for the present system.

We think that one of the largest obstacles to block the direct application of statistical theory to nonrigid molecules lies in the difficulty in ab initio estimate of the absolute value of relevant phase-space volumes and the flux. We therefore study a *nonempirical* method to treat the present evaporation dynamics, nonempirical in that (i) the phase-space volumes and the flux are given on an equal footing and (ii) we do not refer to any other quantities to calibrate or parametrize the values using quantities obtained from experiments and molecular dynamics calculations. We also demand ourselves that (iii) either a harmonic approximation to the global potential energy surface or the rigid body assumption is not used, and (iv) the potential function is not rebuilt so as to reproduce the resultant reaction rate. In this way, we calculate the absolute rate constant and the distribution of released kinetic energy, and compare them with classical trajectory calculations. It is true that statistical theory is empirical in itself and may be further simplified so as to get quick answers in a convenient fashion. However, only after the unbiased numerical realization of a theory, the underlying physical assumption behind the theory can be verified. We hence conceive that these rather precise studies on the methodology should facilitate deeper understanding of the evaporation dynamics of nonrigid clusters.

This paper is organized as follows. Section II shortly describes the system we treat. We show explicitly how evaporation dynamics couples with isomerization. The microcanonical rate constants of evaporation are prepared numerically with molecular dynamics (MD) calculations to verify the statistical theory. In section III we outline the standard version of phase-space theory and its beautiful extension due to Calvo. We then extend this theory to extract the distribution of released kinetic energy after evaporation. Then we consider the practical problems in the applications of the PST in section IV. In section V, the statistical reaction rate and released kinetic energy distribution are examined numerically by comparing with those obtained with MD. The paper concludes in section VI.

II. Molecular Dynamics of Evaporation from a Nonrigid Cluster

This section briefly deals with molecular dynamics of evaporation from an Ar_8-like cluster. We first confirm the evaporation certainly couples with structural isomerization and then estimate the microcanonical reaction (evaporation) rates.

These data will serve as references to examine the statistical theory.

A. Ar_8-Like System. The Hamiltonian we use is

$$H = \frac{m}{2}\sum_{i=1}^{8}\left[\left(\frac{dx_i}{dt}\right)^2 + \left(\frac{dy_i}{dt}\right)^2 + \left(\frac{dz_i}{dt}\right)^2\right] + \sum_{i<j} V(r_{ij}) \qquad (1)$$

with the obvious notations for masses, momenta, and the internuclear distances. The potential function $V(r_{ij})$ we adopt is the pairwise Morse potential defined as

$$V(r_{ij}) = \epsilon[e^{-2\beta(r_{ij}-r_0)} - 2e^{-\beta(r_{ij}-r_0)}] \qquad (2)$$

By the following transformations

$$\tilde{r}_{ij} = \frac{r_{ij}}{r_0} \qquad \tilde{x}_i = \frac{x_i}{r_0} \qquad \tilde{y}_i = \frac{y_i}{r_0} \qquad \tilde{z}_i = \frac{z_i}{r_0}$$

$$\rho_0 = \beta r_0 \qquad \tilde{H} = \frac{H}{\epsilon} \qquad s = \sqrt{\frac{\epsilon}{m{r_0}^2}}t \qquad (3)$$

the Hamiltonian is rewritten in a dimensionless form such that

$$\tilde{H} = \frac{1}{2}\sum_{i=1}^{8}\left[\left(\frac{d\tilde{x}_i}{ds}\right)^2 + \left(\frac{d\tilde{y}_i}{ds}\right)^2 + \left(\frac{d\tilde{z}_i}{ds}\right)^2\right] + \sum_{i<j}(e^{-2\rho_0(\tilde{r}_{ij}-1)} - 2e^{-\rho_0(\tilde{r}_{ij}-1)}) \qquad (4)$$

Thus the Morse potential has only one intrinsic parameter ρ_0 that controls the topography of the potential energy surface. For simplicity, the tildes are omitted in what follows. The values of ρ_0 for selected diatomic molecules, and the related quantities about the time scales, internuclear distances, and energy scales are found in ref 25 (note, however, the scaling parameters in ref 25 are defined in a slightly different way from ours). In this study, ρ_0 is set to 6.0 throughout, which is usually chosen for argon clusters and is similar to the Lennard-Jones potential in topography.

Molecular dynamics for the present system is carried out as follows. The initial configuration was chosen to be the structure of the global minimum potential energy. From this point, each trajectory was launched to a randomly selected direction under a given energy subject to zero total linear and angular momenta. The fourth-order symplectic method[45] was used to integrate the Hamilton canonical equations of motion, with a time step of 10^{-3} (in absolute units according to the dimensionless system in eq 4). The total energy and momentum are conserved within the tolerance of 10^{-7} after the running of 2×10^6 steps, which is equivalent to about 4.72 ns. A thousand trajectories are generated to make an ensemble for each energy.

B. Stable Structures and Quenched Reaction Coordinates for the Evaporation Process. The stable structures of the Ar_8 cluster and their energies are summarized in Figure 1 (left column). It has eight local minima, whose geometries are also displayed. This figure also shows the energy of the lowest transition state (about −18.867) that lies between two DOD structures (permutation isomers). The stable structures of the Ar_7 cluster called PBP, COCT, IST, and SKEW are shown along with their energies in Figure 1 (right column), which are necessary to study the evaporation process from Ar_8.

To energetically connect Ar_8 and (Ar_7 + Ar) on the potential energy surfaces, we here define "quenched reaction coordinates". We begin with the asymptotic limit between an Ar atom and Ar_7 separated as far as 3.43, which is the distance from the center of mass of Ar_7. At this initial configuration, Ar_7 may lie at one of the four possible local minima. The total potential energy goes down as Ar and Ar_7 come closer to each other with an infinitesimal speed (adiabatically), because this is simply a downhill process having no transition state on the potential energy surface. A path starting from this point is tracked with use of the quenching technique,[46] which eventually ends up with one of the eight local minima of Ar_8. This quenched path may be regarded as a reaction coordinate connecting one of the local minima of Ar_7 and that of Ar_8. Some of the similar paths thus obtained are exhibited in Figure 2. Because each cluster has several isomers, many quenched reaction coordinates connecting the reactant and product isomers are possible. It is immediately noticed that the correspondence between the isomers of Ar_8 and those of Ar_7 is not one to one. This is because the quenched paths depend on the relative orientation of the initial configuration of (Ar_7 + Ar). Note also that the correspondence is not all-to-all either.

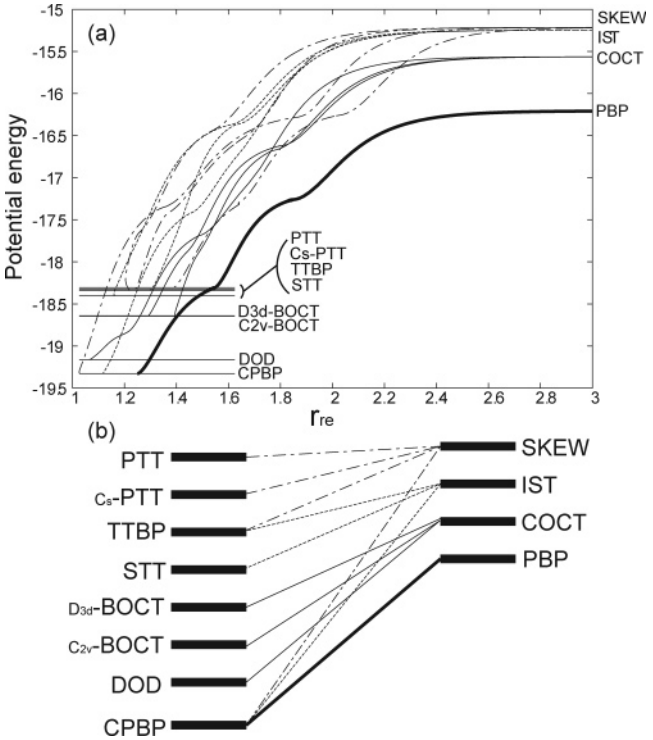

Figure 2. Quenched reaction coordinates (QRC) that connect one of the structures of Ar_8 and one of the structures of Ar_7. (a) The QRC's are projected onto the space of the potential energy and the distance of two fragments. The thickest curve at the bottom represents the minimum energy QRC. (b) shows the outline chart of QRC's. Different types of lines indicate connections to the different isomer of Ar_7.

Obviously these quenched reaction coordinates are different from the widely accepted reaction coordinates like the intrinsic reaction coordinate (IRC)[47] in that the former do not represent the lowest energy path. To find the minimum energy quenched reaction coordinate, we first find the minimum energy orientation between Ar_7 at the bottom of the PBP basin and another Ar atom at the distance of 3.43, and then resume quenching for (Ar_7 + Ar). When a stationary point on the potential is attained, we proceed to the direction of an eigenvector having the smallest (negative) eigenvalue of the locally Hessian matrix of the potential function. We refer the thus obtained path to the minimum energy quenched reaction coordinate. These reaction coordinates will be used later to test the harmonic approximation in statistical theory.

C. Energetic Feature of "Phases". We first summarize the overall feature of the"phase-change" of Ar_8 and Ar_7 as a function of the total energy.

1. "Solid"−"Liquid" Transitions and Nonrigid Clusters. In a low-energy regime, the individual locally stable isomers undergo local small vibration. Without isomerization, the cluster can retain its shape as a "solid" state. As the total energy (E) is raised, some isomerization begins to take place and eventually a large amplitude dynamics due to frequent isomerization results. In this frequent shape-changing stage, the cluster looks like a liquid droplet with high viscosity. The so-called Lindemann index gives a standard way to quantify the transition from the solid-like state to the liquid-like state.[1] The Lindemann index (δ) measures the flexibility of a molecular structure around its average shape. δ for Ar_8 as a function of the total energy shows three "phases" just as other typical cases: (1) the "solid-like" phase with a small and slowly increasing δ below about $E = -17.5$, which is called the "freezing" energy, (2) the "liquid-like" phase with a large and very slowly increasing δ above about $E = -16.0$, called the "melting" energy, and (3) the coexistence region between, where a steep rise of δ is observed. As usual, this behavior of δ is regarded as a prototype of the first-order phase transition. Ar_8 also undergoes frequent structural transitions above the melting point. In this sense, this molecule is highly nonrigid, and therefore its vibrational and rotational motions can never be separated from each other. On the contrary, an important kinematic force arises from this nonseparable dynamics.[13−16]

2. Evaporation from Cluster. High above the melting energy, evaporation from the cluster begins. Evaporating species are monomer (atomic Ar), dimer (Ar_2), and even larger small clusters. However, the amount of the large species like Ar_3 is actually abundantly small, and therefore we consider only Ar and Ar_2 in molecular dynamics simulation. In Figure 3, the overview of the energetics of the cluster dynamics is schematically summarized for Ar_8 and Ar_7. The lowest potential energy of Ar_7 serves as the minimum energies required for the dissociation of (Ar_7 + Ar). Note, however, the actual massive reactions can take place only with the energies significantly higher that these threshold values. This is because the excess energy is distributed among many other vibrational modes besides the mode of reaction coordinate.

It is natural to expect that evaporation from Ar_8 should be accompanied by the structural isomerization of Ar_8, because the evaporation stage is above the liquidlike state in energy. Besides, Figure 3 suggests that Ar_7 as a product of evaporation may undergo structural isomerization even after the dissociation is over. This is particularly the case for the evaporation of the total energy higher than $E = -12.0$. In such a case it is not meaningful to attempt to identify the individual isomers as a product. For this reason, we do not consider a structure-to-structure (isomer-to-isomer) reaction in this study.

D. Strong Coupling between Evaporation and Isomerization. It is obvious that the dynamics of isomerization and evaporation should couple with each other. An important issue here is the time scale of this coupling. A hope is that an evaporating species leaves so fast that the rest of the cluster seems as though it was frozen during the evaporation process. This situation, if any, may be called the sudden evaporation. We hence survey how often the isomerization takes place during an isomerization. To count the frequency of isomerization, we first define a time, denoted as t_{in}, to be the last time at which the radial component of the relative translational velocity of two dissociating fragments becomes zero (see Figure 4). After

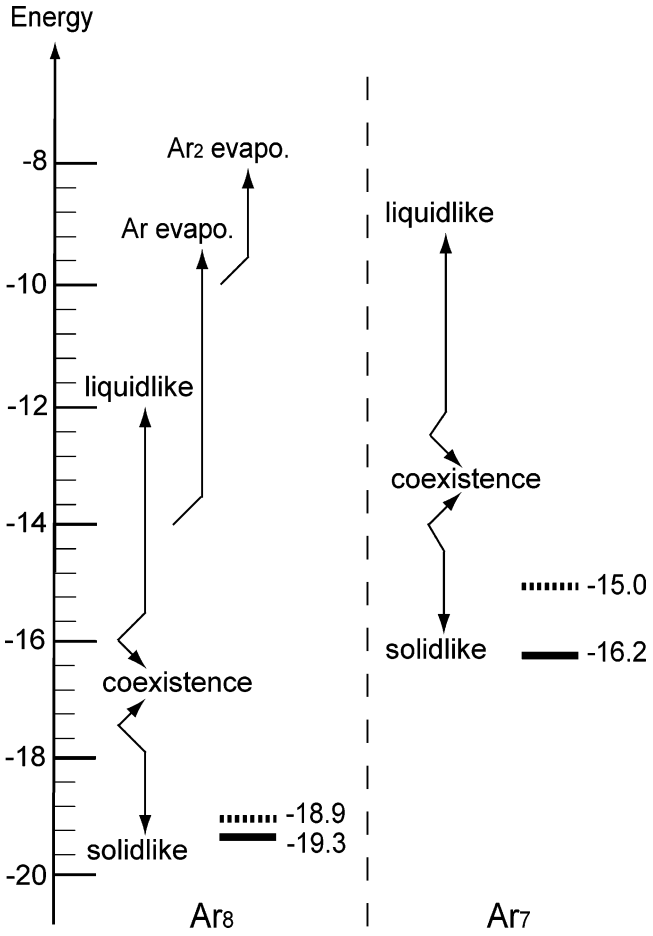

Figure 3. Overview of the energetics of the Morse clusters of Ar_8 and Ar_7. The two heavy lines represent the lowest energy of the isomer of Ar_8 and Ar_7, respectively. The lowest energy of Ar_7 gives a threshold at which monomer evaporation from Ar_8 can take place "theoretically". The two broken heavy lines indicate the lowest transition state energy for the structural isomerization of individual clusters Ar_8 and Ar_7, respectively.

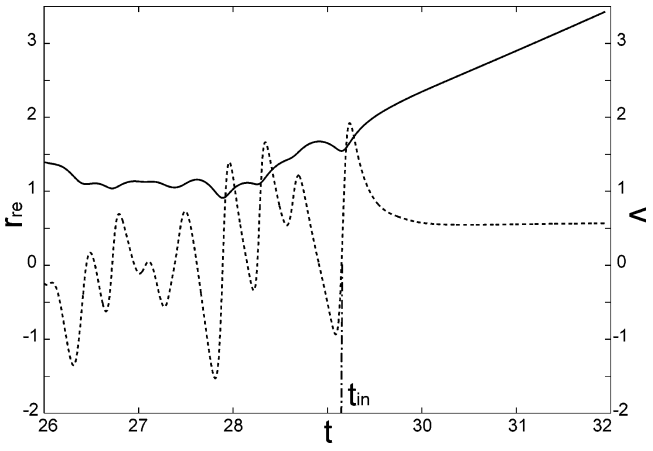

Figure 4. Distance between two fragments Ar_7 and Ar mutually separating (solid curve, scaled to the left axis) and the radial component of the relative translational velocity v between them (dashed curve, scaled to the right axis) as a function of time. Taken from a sampled trajectory for monomer evaporation, whose energy is −10.0. t_{in} represents the last time when the radial component of v becomes zero.

t_{in}, dissociation proceeds with a uniformly positive velocity with no return. In addition, we define t_{out} as a time after which the interaction potential between the fragments becomes as small as −0.01. This situation is usually realized within the relative distance shorter than 2.5 (9.4 Å). [As will be shown later, the

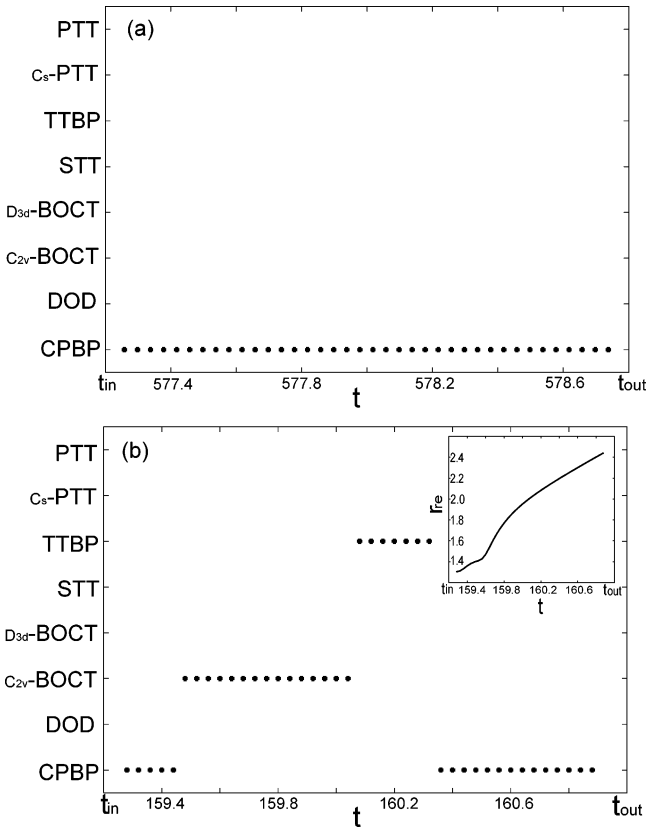

Figure 5. Structural change of the Ar_8 cluster along a trajectory from t_{in} to t_{out}. The vertical axis indicates the names of the possible isomers. (a) For a case where the energy is as low as $E = -13.0$. (b) displays the case of high energy ($E = -10.0$), in which three structural transitions are observed. The inset in (b) shows the distance between two fragments, r_{re}, during the dissociation.

TABLE 1: Probability That the Individual Dissociation Is Accompanied by Isomerization during t_{in} and t_{out}[a]

energy	probability [%]	frequency
−5.0	89.2	3.07
−9.0	76.2	1.69
−13.0	11.0	1.33

[a] Also shown is the average frequency of isomerization in each dissociation event. Three typical energies are sampled.

distance 2.5 is a little further away than the position of the dividing surface at which to calculate the flux.]

We now study the dynamics of isomerization during the time interval from t_{in} to t_{out}. Recall that before t_{in} Ar_8 repeats isomerization frequently because it is already in the "liquid-like" phase. Incidentally, structural change is identified with the so-called quenching technique.[46] Figure 5 shows two examples of structural transition during t_{in} and t_{out}. Panel (a) is for low energy and (b) is for a case of high energy. As can be seen in (b), isomerization takes place a couple of times during the relevant interval. That is, the dissociation and isomerization are not independent but have a strong correlation, which cannot be approximated by the sudden evaporation model. Indeed, Table 1 shows quantitatively how frequently the individual dissociation is accompanied by isomerization during t_{in} and t_{out}. This table also shows the average frequency of isomerization in each dissociation event. These results clearly demonstrate that structural isomerization actually occurs while a receding species is on the way toward separation yet within the interaction region. This is a crucial factor that any statistical theory should take into account.

E. Energy-Resolved Rate Constants of Evaporations with Molecular Dynamics. We here evaluate the reaction rates for monomer and dimer evaporation. Prepare a microcanonical ensemble of Ar_8 clusters. Then they will decay to Ar_7 or Ar_6. If there are a pair of atoms whose mutual distance is shorter than 1.5 after a long time passes from t_{in}, we regarded them as a diatomic molecule leaving Ar_6 behind (dimer evaporation). We neglect the further reaction, if any, for the products Ar_7 or Ar_6 to proceed to the next products. Therefore we do not consider successive reactions like $Ar_8 \rightarrow Ar_7 + Ar \rightarrow Ar_6 + 2Ar$. Let $N_8(t)$, $N_7(t)$, and $N_6(t)$ be the numbers of Ar_8, Ar_7, and Ar_6, respectively, at time t. Also, denote k_{87} and k_{86} as the rate for Ar_8 to change to Ar_7 and Ar_6, respectively. Then the rate equations should be given as

$$\frac{dN_8(t)}{dt} = -k_{87}N_8(t) - k_{86}N_8(t) \quad (5)$$

$$\frac{dN_7(t)}{dt} = k_{87}N_8(t) \quad (6)$$

$$\frac{dN_6(t)}{dt} = k_{86}N_8(t) \quad (7)$$

and the solutions are readily obtained as $N_8(t) = -N_8(0)\exp\{-(k_{87} + k_{86})t\}$, $N_7(t) = N_8(0)k_{87}/(k_{87} + k_{86})[1 - \exp\{-(k_{87} + k_{86})t\}]$, and $N_6(t) = N_8(0)k_{86}/(k_{87} + k_{86})[1 - \exp\{-(k_{87} + k_{86})t\}]$.

Calculating the number $N_8(t)$ in an ensemble of trajectories is equivalent to measuring the lifetime distribution of Ar_8 for an individual trajectory. Here we use t_{in} as the definition of lifetime of Ar_8. Likewise, we count $N_8(t)$, $N_7(t)$, and $N_6(t)$. With the least-square fitting we have calculated $k_{87} + k_{86}$, $k_{87}/(k_{87} + k_{86})$, and $k_{86}/(k_{87} + k_{86})$, which are sufficient to reproduce k_{87} and k_{86}. Note that k_{87} and k_{86} can be obtained independently in a single set of MD calculations. However, this paper compares only k_{87} and will be summarized later in Figure 8 along with the statistically given k_{87}.

To examine the dependence of the rate constants thus evaluated on the preparation of the initial microcanonical ensemble, we carried out the similar calculations with another sampling as follows. (i) Prepare atomic positions randomly in configuration space. This random "molecule" usually has a very high energy. (ii) Quench this molecule adiabatically down to the point at which the potential energy becomes equal to a total energy aimed. Thus, the quenched molecule is therefore at a turning point. (iii) Let it run with the zero initial momentum. This sampling and the one described in section IIA constitute the opposite extremes: In the former, the initial momentum is zero (all the initial energy is concentrated to the potential energy), whereas for the latter the initial potential energy is zero (all the initial energy is concentrated to the kinetic energy). Nevertheless, the rate constants evaluated with these ensembles have shown a very good agreement. This is presumably because the system has sufficiently a long induction time before evaporation takes place, during which it undergoes isomerization many times to visit the possible isomers in an ergodic manner.

III. Phase-Space Theory for Molecular Evaporation

We first outline the standard form of phase-space theory (PST) along with its limitation in treating the cluster evaporation. Then we proceed to the sophisticated version of phase-space theory developed mainly by Calvo and his co-workers, with which we study the dissociation dynamics of nonrigid molecules.

Finally, the statistical expression of kinetic energy distribution due to evaporation is discussed.

A. Standard PST Scheme Assuming the Separation of Rotational and Vibrational Motions. *1. Separation of Vibrational and Rotational Modes.* phase-space theory[48] expresses the microcanonical rate constant for dissociation reaction as the ratio of a flux flowing out across a dividing surface to the possible population inside this surface. More explicitly, it is

$$k(E,\mathbf{J}) = \frac{W(E,\mathbf{J})}{\Omega(E,\mathbf{J})} \tag{8}$$

where $W(E,\mathbf{J})$ is the flux across the dividing surface toward a product channel and $\Omega(E,\mathbf{J})$ is the volume of classical phase space assigned to a reactant region (inside the dividing surface). $\mathbf{J}$ collectively represents the conservatives arising from the symmetry of a system such as the total angular momentum. The theory is quite general as long as the background statistical hypothesis is valid. Nevertheless, in actual applications, one cannot help introducing further approximations depending on a system under study. In particular, to apply this theory successfully, it is very critical where to locate the dividing surface, in addition to accurate estimates of $W(E,\mathbf{J})$ and $\Omega(E,\mathbf{J})$.

It is a standard practice to assume the separation of vibrational and rotational modes in an application of PST to a "tight" chemical reaction, in which the system does not undergo a large structural change. Under this assumption, $W(E,\mathbf{J})$ is represented in a form of convolution of the density of states for rotational and vibrational modes, e.g., $W_{\mathrm{rot.}}$ and Ω_{vib}, respectively, in such a way that

$$W(E,\mathbf{J}) = \int_{E^*_{\mathrm{rot}}(\mathbf{J})}^{E-E_0} \mathrm{d}E_{\mathrm{rot.}}\, W_{\mathrm{rot.}}(E_{\mathrm{rot.}},\mathbf{J})\, \Omega_{\mathrm{vib}}(E-E_0-E_{\mathrm{rot.}}) \tag{9}$$

where $\Omega_{\mathrm{vib}}(E - E_0 - E_{\mathrm{rot.}})$ is the vibrational density of states at a dividing surface, E_0 is the potential energy of the dividing surface, $E^*_{\mathrm{rot.}}(\mathbf{J})$ is the minimum energy required to reproduce the angular momentum $\mathbf{J}$, and $W_{\mathrm{rot.}}(E_{\mathrm{rot.}},\mathbf{J})$ is the number of rotational-orbital states at the dividing surface with their energies less than or equal to $E_{\mathrm{rot.}}$, which is the sum of translational and rotational energies at the dividing surface. General expressions for calculating $W_{\mathrm{rot.}}(E_{\mathrm{rot.}},\mathbf{J})$ have been discussed in refs 40 and 48. Recall that rigid body rotation has to be assumed to estimate $W_{\mathrm{rot.}}(E_{\mathrm{rot.}},\mathbf{J})$ of eq 9 at a given rotational energy, which freezes the degrees of freedom for the change of molecular "shapes".

2. Phase-Space Volume $\Omega(E,\mathbf{J})$ Assuming Harmonic Vibrations. To attain a rough estimate of the phase-space volume for a single basin problem as in a simple chemical reaction, it is a usual practice that the true potential function is approximated in terms of the harmonic oscillators.[49] Although useful, this approximation should be totally invalid in our multibasin dynamics. In their studies of chaos, Reinhardt and his coworkers[43,44] developed the so-called adiabatic switching method to estimate the phase-space volume by adiabatically deforming a potential function starting from an approximate reference oscillator to the actual one at hand. Weerasinghe and Amar[32] applied this method to argon clusters using the coupled harmonic oscillators as a reference potential. The notion of adiabatic switching is based on an observation by Hertz[50] that the phase-space volume enclosed by an isoenergetic shell (classical sum of states) is an invariant with respect to adiabatic modification of the Hamiltonian. However, the classical adiabatic theorem essentially rests on the continuous and smooth (adiabatic) change of the phase-space structure due to, for instance, ergodicity,[51] and therefore the sudden change of the phase-space feature is quite likely to break the theoretical ground.[52,53] It is therefore quite questionable for this theorem to be valid in the case where the adiabatic switching changes the relevant dynamics from chaos to regular motion, or vice versa, because the dimensionality of phase-space for a completely chaotic motion to occupy is $2n - 1$, whereas that of the completely integrable counterpart is n, where $2n$ is the dimension of phase-space. We hence need a practical yet accurate method to estimate the phase-space volumes for the present system.

B. Extended Phase-Space Theory of Calvo and Labastie:[35] Treatment of **Dissociation Reaction for Nonrigid Systems.** The microcanonical rate constant for unimolecular dissociation of an energy E, total linear momentum $\mathbf{P}$, and total angular momentum $\mathbf{J}$, is given by

$$k(E,\mathbf{P},\mathbf{J}) = \frac{W(E,\mathbf{P},\mathbf{J})}{\Omega(E,\mathbf{P},\mathbf{J})} \tag{10}$$

where $W(E,\mathbf{P},\mathbf{J})$ is the flux across the dividing surface and $\Omega(E,\mathbf{P},\mathbf{J})$ is the initial phase-space volume to be estimated under these conditions.[54] For a cluster composed of N identical atoms, they are formally expressed as

$$\Omega(E,\mathbf{P},\mathbf{J}) = \int\prod_{i=1}^{N} \mathrm{d}\mathbf{r}_i\, \mathrm{d}\mathbf{p}_i\, \delta[H(\{\mathbf{r}_i\},\{\mathbf{p}_i\}) - E]\, \delta[\sum_{i=1}^{N}\mathbf{p}_i - \mathbf{P}]\, \delta[\sum_{i=1}^{N}\mathbf{j}_i - \mathbf{J}]$$

and

$$W(E,\mathbf{P},\mathbf{J}) = D_g\int\prod_{i=1}^{N} \mathrm{d}\mathbf{r}_i\, \mathrm{d}\mathbf{p}_i\, \delta[H(\{\mathbf{r}_i\},\{\mathbf{p}_i\}) - E]\, \delta[\sum_{i=1}^{N}\mathbf{p}_i - \mathbf{P}]\, \delta[\sum_{i=1}^{N}\mathbf{j}_i - \mathbf{J}]\, \delta[r_{\mathrm{re}} - r^{\ddagger}_{\mathrm{re}}]\dot{r}_{\mathrm{re}} \tag{11}$$

where D_{g} is the degeneracy of the dissociative atom, $\mathbf{j}_i$ is the angular momentum of the ith atom ($\mathbf{j}_i = \mathbf{r}_i \times \mathbf{p}_i$), r_{re} is the distance between the center of mass of two fragments, and $r^{\ddagger}_{\mathrm{re}}$ denotes the position of the dividing surface, which will be specified later. The relevant integration over the momentum space can be performed analytically without the separation of vibrational and rotational motions, which gives rise to

$$\Omega(E,\mathbf{P},\mathbf{J}) = \frac{(2\pi)^{s/2}}{\Gamma\left(\frac{s}{2}\right)N^{3/2}}\int\prod_{i=1}^{N}\frac{\mathrm{d}\mathbf{r}_i}{\sqrt{\det I_N(\{\mathbf{r}_i\})}}\left(E - V(\{\mathbf{r}_i\}) - \frac{\mathbf{P}^2}{2N} - (\mathbf{J}-\mathbf{J}_{\mathrm{c}})^{\mathrm{T}}\frac{I_N^{-1}(\{\mathbf{r}_i\})}{2}(\mathbf{J}-\mathbf{J}_{\mathrm{c}})\right)^{(s-2)/2} \tag{12}$$

and

$$W(E,\mathbf{P},\mathbf{J}) = \frac{D_{\mathrm{g}}(2\pi)^{(s-1)/2}}{\Gamma\left(\frac{s+1}{2}\right)N^{3/2}\sqrt{m_{\mathrm{r}}}}\int\prod_{i=1}^{N}\frac{\mathrm{d}\mathbf{r}_i}{\sqrt{\det I_N(\{\mathbf{r}_i\})}}\delta[r_{\mathrm{re}} - r^{\ddagger}_{\mathrm{re}}]\left(E - V(\{\mathbf{r}_i\}) - \frac{\mathbf{P}^2}{2N} - (\mathbf{J}-\mathbf{J}_{\mathrm{c}})^{\mathrm{T}}\frac{I_N^{-1}(\{\mathbf{r}_i\})}{2}(\mathbf{J}-\mathbf{J}_{\mathrm{c}})\right)^{(s-1)/2} \tag{13}$$

where $\mathbf{J}_c$ is the angular momentum of the center of mass moving with respect to the space fixed frame. On the other hand, I_N is the 3×3 tensor of inertia in the frame of the center of mass, m_r is the reduced mass of the two fragments, and $s = 3N - 6$ is the internal degrees of freedom. These formulas are essentially the same as those derived by Calvo and Labastie,[35] although the expression eq 13 is not seen in the literature. The details of these integrals over the momentum space are described in the appendix.

One can always set $\mathbf{P} = 0$ without loss of generality. In addition, locating the origin of the space fixed frame at the center of mass of a system, one can also choose as $\mathbf{J}_c = 0$. Further, as in the MD simulation in the preceding section, we study only the case of $\mathbf{J} = 0$. The phase-space volume Ω and flux W are then represented as a convolution between the configuration space term and the momentum space term, denoted by the subscript Q and P , respectively as

$$W(E) = \int_0^E \mathrm{d}\epsilon\, \Omega_Q^{\ddagger}(\epsilon)\, W_P(E-\epsilon) \tag{14}$$

and

$$\Omega(E) = \int_0^E \mathrm{d}\epsilon\, \Omega_Q(\epsilon)\, \Omega_P(E-\epsilon) \tag{15}$$

where

$$\Omega_Q(\epsilon) = \frac{1}{8\pi^2 N!}\frac{1}{N^{3/2}}\int\prod_{i=1}^{N-1}\mathrm{d}r_i\,\frac{\delta[\epsilon - V(\{\mathbf{r}_i\})]}{\sqrt{\det I_N(\{\mathbf{r}_i\})}} \tag{16}$$

$$\Omega_Q^{\ddagger}(\epsilon) = \frac{1}{8\pi^2 N!}\frac{D_g}{N^{3/2}\sqrt{m_r}}\int\prod_{i=1}^{N-1}\frac{\mathrm{d}\mathbf{r}_i}{\sqrt{\det I_N(\{\mathbf{r}_i\})}}\delta[r_{re} - r_{re}^{\ddagger}]\delta[\epsilon - V(\{\mathbf{r}_i\})] \tag{17}$$

$$\Omega_P(E-\epsilon) = \frac{(2\pi)^{s/2}}{\Gamma\left(\frac{s}{2}\right)}(E-\epsilon)^{(s-2)/2} \tag{18}$$

and

$$W_P(E-\epsilon) = \frac{(2\pi)^{(s-1)/2}}{\Gamma\left(\frac{s+1}{2}\right)}(E-\epsilon)^{(s-1)/2} \tag{19}$$

In these expressions, $\Omega_Q(\epsilon)$ denotes the volume of configuration space belonging to a given potential energy ϵ, $\Omega_Q^{\ddagger}$ is the configuration-space volume of ϵ in the dividing surface (actually many-dimensional manifold), $\Omega_P(E-\epsilon)$ is the momentum space volume for the kinetic energy $E - \epsilon$, $W_P(E-\epsilon)$ is the volume of the momentum space accumulated up to $E - \epsilon$ (corresponding to the number of states), and the term $1/8\pi^2 N!$ is a factor to take account of the rotational and permutation symmetries of the particles. Thus the final form of the rate expression is reduced to

$$k(E) = \frac{\int_0^E \mathrm{d}\epsilon\, \Omega_Q^{\ddagger}(\epsilon)\, W_P(E-\epsilon)}{\int_0^E \mathrm{d}\epsilon\, \Omega_Q(\epsilon)\, \Omega_P(E-\epsilon)} \tag{20}$$

Because the momentum-space terms have been given analytically, the estimate of $k(E)$ amounts essentially to the calculations of $\Omega_Q^{\ddagger}(\epsilon)$ and $\Omega_Q(\epsilon)$, which will be our main task in the next section. We emphasize again that the above statistical expression for dissociation rate is general enough to apply to a system that undergoes a large change of molecular shape like our cluster dynamics, for which separation of vibrational and rotational is far from the reality.

Some remarks with respect to eqs 14−20 are in order. (1) If the harmonic approximation is applied to the flux eq 14 and the phase-space volume eq 15 as well, they are represented in the well-known forms

$$W_h(E) = \frac{(E - E^{\ddagger})^{s-1}}{\Gamma(s)\prod_{k=1}^{s-1}\nu_k^{\ddagger}} \tag{21}$$

$$\Omega_h(E) = \frac{E^{s-1}}{\Gamma(s)\prod_{k=1}^{s}\nu_k} \qquad s = 3N - 6 \tag{22}$$

where $\nu_k^{\ddagger}$ ($k = 1, ..., s - 1$) are the frequencies of the normal modes orthogonal to the minimum energy quenched reaction coordinate (see section IIB), $E^{\ddagger}$ is the potential energy at the dividing surface, ν_k ($k = 1, ..., s$) are the frequencies of the normal modes at the global minimum, and $\Gamma(s)$ is the Gamma function. The reaction rate is given as

$$k_h(E) = \frac{W_h(E)}{\Omega_h(E)} \tag{23}$$

These harmonic approximations are numerically realized in the next section. (2) It has been found that the total phase-space volume in the form of the convolution between the volumes in momentum and configuration spaces, eq 15, can be used to define a temperature in a microcanonical ensemble, called the microcanonical temperature, which turns out to characterize the isomerization dynamics of cluster M_7 very well.[11] (3) The presence of the factor $1/\sqrt{\det I_N(\{\mathbf{r}_i\})}$ in $\Omega_Q(\epsilon)$ and $\Omega_Q^{\ddagger}(\epsilon)$, which is reduced to $1/I_N$ in the case of linear molecules, was previously established in terms of the principal momenta of inertia by several authors.[41,42,55,56] In transforming from the $3N$-dimensional isotropic Euclidean space to the $(3N - 6)$-dimensional internal molecular space (or molecular shape space), the factor $1/\sqrt{\det I_N(\{\mathbf{r}_i\})}$ disappears, and at a price the metric term appears. Indeed, Teramoto and Takatsuka have explicitly shown the effects of the metric of the molecular shape space.[16] Besides, it has been revealed by Yanao and Takatsuka that this metric (or the intrinsic curvature of the space) gives rise to an important kinematic force that can strongly affect the shape-changing dynamics of molecules.[13−15]

C. Kinetic Energy Release (KER). We next extend the phase-space-volume formula of Calvo and Labastie[35] for a prediction of the final distribution of released kinetic energy. We consider only the monomer evaporation ($Ar_N \rightarrow Ar_{N-1} + Ar$). KER is defined as follows: The kinetic energy at the dividing surface is divided as

$$\frac{1}{2}m_r\dot{r}_{re}^{\,2} + \frac{1}{2}\mathbf{L}^{\mathrm{T}}{I_L}^{-1}\mathbf{L} + \frac{1}{2}\mathbf{J}_{N-1}^{\mathrm{T}}{I_{N-1}}^{-1}\mathbf{J}_{N-1} \tag{24}$$

where m_r, I_L, and $\mathbf{L}$ represent the reduced mass, the inertial tensor, and the orbital angular momentum of two fragments. $\mathbf{J}_{N-1}$ and I_{N-1} represent the angular momentum and the inertial tensor of the Ar_{N-1} with respect to the center-of-mass of the

Ar_{N-1}. The kinetic energy released is the sum of the translational energy and the rotational energies. The flux at the dividing surface, eq 11, is also distributed according to the KER, so that the (unnormalized) probability density for the KER is represented as

$$P_u(E,\epsilon_K) = D_g \int \prod_{i=1}^{N} d\mathbf{r}_i\, d\mathbf{p}_i\, \delta[\sum_{i=1}^{N}\mathbf{r}_i]\, \delta[\sum_{i=1}^{N}\mathbf{p}_i]\, \delta[\sum_{i=1}^{N}\mathbf{j}_i]\, \delta[E - H(\{\mathbf{r}_i\},\{\mathbf{p}_i\})]\, \delta[r_{re} - r_{re}^{\ddagger}]\dot{r}_{re}\, \delta\left[\epsilon_K - \left(\frac{1}{2}m_r\dot{r}_{re}^{\,2} + \frac{1}{2}\mathbf{L}^T I_L^{\,-1}\mathbf{L} + \frac{1}{2}\mathbf{J}_{N-1}^T I_{N-1}^{\,-1}\mathbf{J}_{N-1}\right)\right] \quad (25)$$

where we have set $\mathbf{P} = \mathbf{J} = \mathbf{0}$, and the center of mass is located at the origin of the coordinate system. Integrating out the kinetic part leads to

$$P_u(E,\epsilon_K) = \int_0^{E-\epsilon_K} d\epsilon\, \Omega_Q^{\ddagger}(\epsilon)\, \Omega_{P;N-1}(E-\epsilon-\epsilon_K)\, W_r(\epsilon_K) \quad (26)$$

where $\Omega_{P;N-1}$ is the momentum-space density of states of the vibrational motion of the Ar_{N-1}, which is explicitly written as

$$\Omega_{P;N-1}(x) = \frac{(2\pi)^{\tilde{s}/2}}{\Gamma(\tilde{s}/2)} x^{(\tilde{s}-2)/2} \qquad \tilde{s} = 3(N-1) - 6$$

and W_r is the momentum-space sum of states of the rotational motion of the two fragments, that is

$$W_r(x) = 2\pi x \quad (27)$$

The derivation of eq 26 is shown in Appendix. Thus the normalized probability density is represented as

$$P(E,\epsilon_K) = P_u(E,\epsilon_K)/W(E) \quad (28)$$

with

$$W(E) = \int d\epsilon_K\, P(E,\epsilon_K) \quad (29)$$

Formulating these expressions seems to be rather straightforward, but applying them is highly nontrivial. Indeed, to the best of our knowledge, KER in the literature has been calculated by means of more conventional models and/or limited methods imposing various assumptions. We shall carry out the full nonempirical statistical calculations of KER in section V.

IV. Practices To Evaluate the Statistical Rates

We here study how the statistical theories above are materialized numerically. This aspect is crucial for the practical applications of the theories.

A. Absolute Value of Phase-Space Volume for Many-Dimensional Systems. The calculations of phase-space volume and its related quantities always constitute a crucial key to practical applications of statistical theories. For instance, in the study of cluster isomerization dynamics, Seko and Takatsuka[5,6] developed an efficient algorithm to generate random configurations of a cluster in estimating the phase-space volume to be assigned to individual potential basins (corresponding to the isomers). However, only the calculation of the relative phase-space volumes of individual basins was enough in those studies, because the rate of isomerization was the central concern there. However, the absolute values of phase-space volume is necessary for the present evaporation dynamics.

The basic quantity to be determined here is $\Omega_Q(\epsilon)$ (volume in configuration space belonging to a potential energy ϵ) in eq 16, because the volume in momentum space is already given analytically. To estimate $\Omega_Q(\epsilon)$ in eq 16, we set the origin of the coordinate at the position of the Nth atom in such a way that

$$\Omega_Q(\epsilon) = \frac{1}{8\pi^2 N!}\frac{1}{N^{3/2}} \int d\mathbf{r}_{1,N} \cdots d\mathbf{r}_{N-1,N} \frac{\delta[\epsilon - V(\{\mathbf{r}_{i,N}\})]}{\sqrt{\det I_N(\{\mathbf{r}_{i,N}\})}} \quad (30)$$

where $\mathbf{r}_{i,N}$ is the position vector $\mathbf{r}_{i,N} = \mathbf{r}_i - \mathbf{r}_N$. As usual, we have no practical way to estimate this multidimensional (21 for $N = 8$) integral other than the Monte Carlo technique. We thus generate a set of random numbers, e.g., S, to represent many configurations $\{\mathbf{r}_{1,N}, \mathbf{r}_{2,N}, ..., \mathbf{r}_{N-1,N}\}$. All the members of S are generated so that their given potential energies do not exceed the maximum value of our concern (the maximum potential value is set to 20.0). Also, the sampled points should lie inside the dividing surface. With use of the sampling points generated above, $\Omega_Q(\epsilon)$ is rewritten as

$$\Omega_Q(\epsilon) \simeq \frac{1}{8\pi^2 N!} \sum_{s_i \in S} \frac{\delta_{nu}[V(\{\mathbf{r}_{i,N}\}) - \epsilon]}{\sqrt{\det I_N}} \Delta \quad (31)$$

where the δ function is approximated in terms of a sharp pulse function of the rectangular form (denoted as δ_{nu}), and Δ is the measure (weighting factor) to perform the integration, which is actually the function of a sampling set S.

However, because the measure is scarcely known in practice, the standard way to eliminate Δ is to divide the number of sampling points that satisfy the condition of the integrand to the total number of sampling points generated (note that a random sampling in the functional space is required in addition to the random generation of the coordinate points $\{\mathbf{r}_{i,N}\}$). Indeed, the number of those points that fall into the range of the nonzero value of the δ function (actually δ_{nu}) in the entire sampling space is very small practically, and therefore a large fluctuation in this procedure makes it extremely hard to give a reasonable estimate of the integral. Under this situation, in which the computation of the function V in the δ function is also time-consuming, the evaluation of the measure Δ is far more preferable in the aspect of both accuracy and computational time to increasing the size of Monte Carlo sampling to an astronomical scale. We hence devise a method to figure out the value of Δ below.

In the spirit of the Monte Carlo method, we assume that Δ is uniform (constant) over the entire space. We first consider the following integral

$$\omega^N(e_1,...,e_{N-1}) = \int d\mathbf{r}_{1,N} \cdots d\mathbf{r}_{N-1,N}\, \delta[V(\mathbf{r}_{1,N}) - e_1] \cdots \delta[V(\mathbf{r}_{N-1,N}) - e_{N-1}] \quad (32)$$

which is similar to eq 30, yet ω^N is simply a direct product of the integrals for three-dimensional δ functions. Hence, it can be analytically performed, resulting in

$$\omega^N(e_1,...,e_{N-1}) = \prod_{i=1}^{N-1} \int d\mathbf{r}_{i,N}\, \delta[V(\mathbf{r}_{i,N}) - e_i] = \prod_{i=1}^{N-1} \Omega_Q^{(2)}(e_i) \quad (33)$$

where

$$\Omega_Q^{(2)}(e) = \int \mathrm{d}x\, \mathrm{d}y\, \mathrm{d}z\, \delta[e - V(x,y,z)] \tag{34}$$

This quantity is analytically given as

$$\Omega_Q^{(2)}(e) = \frac{-4\pi}{2\rho_0\alpha(\alpha-1)}\left[\frac{2\alpha}{\rho_0}\ln\left(\frac{1+\sqrt{\alpha}}{1-\sqrt{\alpha}}\right) + \frac{\alpha}{{\rho_0}^2}\ln\left(\frac{1-\sqrt{\alpha}}{1+\sqrt{\alpha}}\right)\ln(1-\alpha) + 2\sqrt{\alpha} - \frac{2\sqrt{\alpha}}{\rho_0}\ln(1-\alpha) + \frac{\sqrt{\alpha}}{{\rho_0}^2}\{\ln^2(1-\sqrt{\alpha}) + \ln^2(1+\sqrt{\alpha})\}\right] \tag{35}$$

with $\alpha = 1 + e$ for the Morse potential. On the other hand, one can deliberately estimate $\omega^N(e_1,...,e_{N-1})$ with the Monte Carlo method using the same sampling set S as above, that is

$$\omega^N(e_1,...,e_{N-1}) \simeq \sum_{s_i \in S}\left(\prod_{i=1}^{N-1}\delta_{\mathrm{nu}}[V(\mathbf{r}_{i,\mathrm{N}}) - e_i]\right)\Delta \tag{36}$$

where the δ function is also approximated in the same way as above. Comparing the rigorous result of eq 33 and that estimated with eq 36, one can determine Δ. Because Δ thus obtained numerically depends on the choice of $(e_1,...,e_{N-1})$, it is averaged over the $(e_1,...,e_{N-1})$-sampling space. This Δ is brought back into eq 31 to estimate $\Omega_Q(\epsilon)$. To enhance the efficiency of the above Monte Carlo calculations, the Wang−Landau method[57] was applied with the weighting factor $1/\sqrt{\det I_N}$, which is fast and convenient to estimate the configuration-space volume in the wider range of configuration space.

Once the method to calculate the phase-space volume is established, its extension to the calculation of the flux is almost straightforward. We have thus applied the same technique to measure the volume of the dividing surface ($(3N - 7)$-dimensional configurational space). This provides us with a consistent way of the calculations of the phase-space volume of the reactant $\Omega(E)$ and the flux at the dividing surface $W(E)$, which could not be realized before in the study of cluster evaporation dynamics. In Figure 6 we show the absolute value of the flux $W(E)$ and the phase-space volume $\Omega(E)$. For comparison, the results of the harmonic flux $W_\mathrm{h}(E)$ and the harmonic phase-space volume $\Omega_\mathrm{h}(E)$ are also shown in Figure 6 with broken curves. The harmonic phase-space volume $\Omega_\mathrm{h}(E)$ and the harmonic flux $W_\mathrm{h}(E)$ were estimated at the global minimum (CPBP) and on the minimum energy quenched reaction coordinate which connects the CPBP and the PBP, respectively (see eqs 21 and 22). As seen in Figure 6, $\Omega(E)$ and $\Omega_\mathrm{h}(E)$, and $W(E)$ and $W_\mathrm{h}(E)$ as well, in the very low-energy regime agree with each other very well as they should be, which verifies the present method of calculation. In the high-energy region both $\Omega_\mathrm{h}(E)$ and $W_\mathrm{h}(E)$ significantly deviate from $\Omega(E)$, respectively, to the order of 10.[5] This is not surprising, though.

We have been using the Morse potential in this particular study, the analytic functional form of which has been used to calculate $\Omega(E)$ and $W(E)$. However, we often face more general potential functions that are given only numerically or as a fitted function. Yet, their interatomic part (diatomic interaction) is more or less similar to the Morse function. To calculate the density of states for these general potentials, we suggest two ways. The first one is to calculate eq 34 numerically for the actual diatomic interaction, and the same procedure as the present paper should be executed. The other one is to use the adiabatic switching starting from the actual system under study and ending to the Morse cluster.

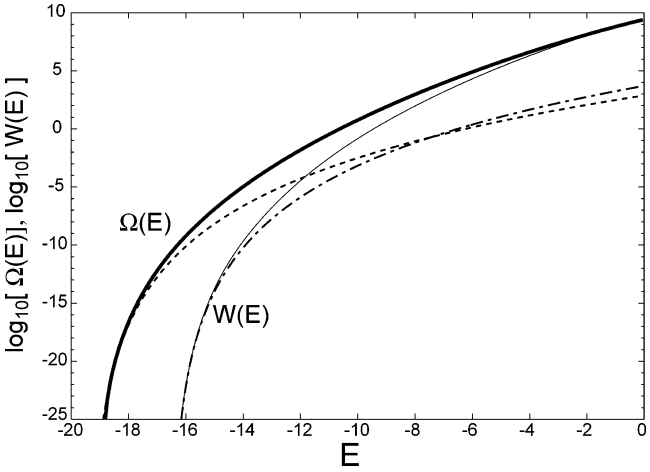

Figure 6. Absolute value of the phase-space volume $\Omega(E)$ (thick solid line) and the flux $W(E)$ (thin solid line). The broken and chained curves represent $\Omega_\mathrm{h}(E)$ and $W_\mathrm{h}(E)$, respectively. $\Omega_\mathrm{h}(E)$ and $W_\mathrm{h}(E)$ were estimated at the global minimum (CPBP) and on the minimum energy quenched reaction coordinate, which connects the CPBP and the PBP, respectively. The distance between two fragments, which is the position of the dividing surface, was set to 2.17 for the calculation of $\Omega(E)$, $W(E)$, and $W_\mathrm{h}(E)$.

B. Determination of the Dividing Surface. Another very critical issue in the application of statistical rate theories is how and where the dividing surface is set. Many studies have been devoted to this problem, such as variational search for the best transition state,[30,58,59] exploring the phase-space structure around a saddle,[60−62] and the formation of an effective potential basin at the transition state due to the non-Euclidean property of molecular internal space.[13−15] The standard transition state theory simply tells us to place a dividing surface at the transition state. However, as far as the present reaction $Ar_8 \rightarrow Ar_7 + Ar$ is concerned, there is no transition state on the potential energy surface, as shown in Figure 2. The centrifugal force may generate an effective barrier, and our theoretical treatment can be applied to such effective transition states. Nevertheless, we do not choose this option in this paper, because (i) we do not consider the angular momentum resolution of the products in the present stage, (ii) the position of the centrifugal barrier depends on the kinetic energy of the relative motion, and (iii) structural isomerization continues even in the area of the centrifugal barrier and therefore the orbital angular momentum continues to couple with the internal rotation and molecular shape of the individual isomers.

Therefore, following the spirit of the variational transition state theories, we set the dividing surface on the basis of the minimum flux criterion;[63] the dividing surface is to be set at the position where the flux $W(E)$ takes the minimum. (Incidentally, we have examined another variational criterion in which the dividing surface is located at a point that gives the minimum reaction rate k. It turns out numerically that these two criteria have not produced significant differences in this system.) The absolute flux was calculated at each position where the distance between two fragments (r_re) are 1.71, 1.83, 1.94, 2.06, 2.17, 2.29, 2.40, and 2.51, which was fitted in an expression $y = \exp(a_3 {r_\mathrm{re}}^3 + a_2 {r_\mathrm{re}}^2 + a_1 r_\mathrm{re} + a_0)$ to deduce the minimum flux point. This fitted curve is usually convex downward and consequently has a minimum within the domain of r_re we scanned. We carried out this procedure for the individual total energies of our concern. Figure 7 shows an example of the flux against the distance between two fragments (r_re) at the $E =$

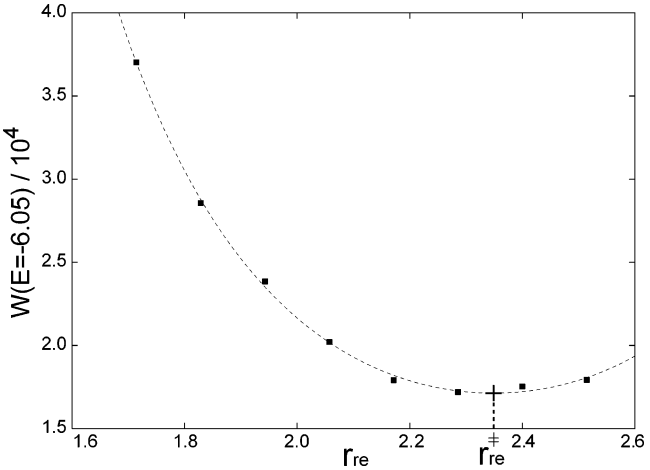

Figure 7. Variational behavior of the flux as a function of the distance from Ar_7 (r_{re}). Dots represent the absolute value of the flux $W(E)$ versus the distance between Ar and Ar_7. The broken curve is obtained with the least-squares method. The cross represents the minimum flux point. The total energy of the cluster is −6.05.

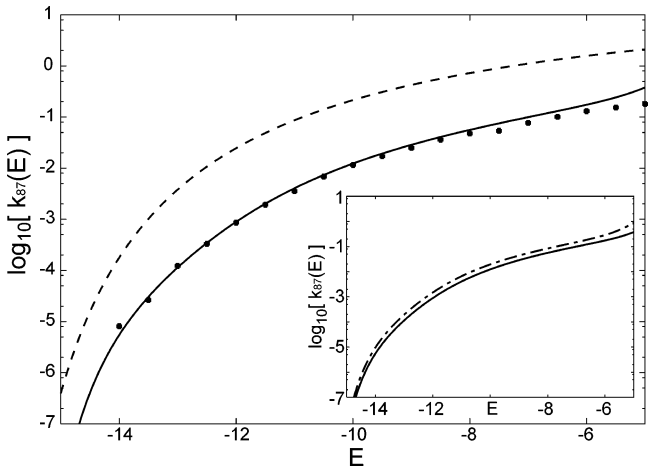

Figure 8. Rate constants versus the total energy E for the monomer evaporation from Ar_8. Dots are the results obtained from the classical trajectory calculations, and smooth curves result from the present statistical treatment. The ratio of the latter to the former is typically about 1.1. The broken line represents the rate given by the harmonic approximation. In the inset, a statistical rate that neglects the factor $\sqrt{\det I_N(\{\mathbf{r}_i\})}$ (chain curve) is compared with the full statistical rate (solid curve). The former consistently overestimates the true one by the factor 1.4−1.8.

−6.05. The minimum flux positions thus determined are used to estimate the reaction rates.

V. Numerical Results for Monomer Evaporation

We are now at the point where the theories and numerical algorithms should be examined numerically in a nonempirical manner. We here consider only monomer evaporation in both the statistical and the MD treatments.

A. Reaction Rates. With the statistical method developed above, we have calculated the rate constants (denoted as k_{87}^{st}) for the monomer (atomic) evaporation from Ar_8. The evaporation rate constants are now compared with k_{87} (denoted as k_{87}^{MD}) obtained in section IIE with molecular dynamics, which are shown altogether in Figure 8. Agreement between them is very good. $k_{87}^{MD}/k_{87}^{st} = 1.30, 1.06, 1.08$ at the total energy $E = -7.0$, -10.0, -13.0, respectively. In view of the use of the Monte Carlo technique, we are not eligible to claim more. Nevertheless,

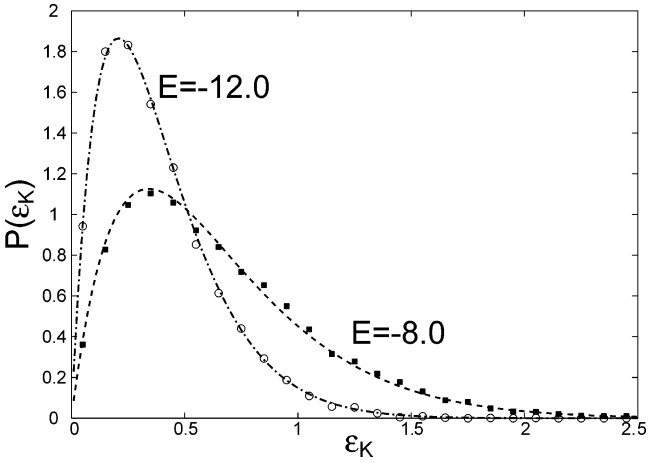

Figure 9. Probability distribution of the released kinetic energy after the monomer evaporation at $E = -12.0$ and -8.0. The chained and broken curves represent the statistical results. Dots represent the molecular dynamics values.

the present results demonstrate that the statistical theory can work extremely well and the underlying physical assumption to describe evaporation from a nonrigid molecule reflects the true dynamics faithfully.

The accuracy of the statistical rate tends to be deteriorated in the energy above ca. −8. Looking back at Figure 3, we notice that dimer evaporation $Ar_8 \rightarrow Ar_6 + Ar_2$ may take place rather massively at this energy. It is indeed the case.[27] On the other hand, the present variational calculation of the dividing surface rests on the monomer evaporation. Therefore, the slight discrepancy between the statistical and MD results in the high-energy region suggests that the variational calculation should be performed with respect to the total flux of Ar and Ar_2 evaporations. This aspect requires further study, which is beyond the scope of this paper.

We have also shown the rate constant obtained by the harmonic approximation, namely, eq 23. The harmonic results are consistently larger than the full statistical values by 10−100 times. However, it is a nice feature that qualitative behavior of the rate is mostly parallel with the full statistical values over the wide range of energy. This finding is never trivial. On the contrary, it is surprising, if we recall the energy dependence of $\Omega_h(E)$ and $W_h(E)$ in Figure 6. Both deviate individually more and more from the full statistical counterparts, namely, $\Omega(E)$ and $W(E)$, as E is increased. But Figure 8 suggests that the errors in $\Omega_h(E)$ and $W_h(E)$ are balanced well enough to give such a parallel behavior.

Finally, we numerically examine the effect of the tensor of inertia, actually, in the form $\det I_N(\{\mathbf{r}_i\})$ of eqs 12 and 13. Omitting the factor $\sqrt{\det I_N}$ in the calculation of $\Omega(E)$ leads to overestimation by a factor of about 10^2 in the present system. Likewise a similar omission from $W(E)$ overestimates it. However, again, the errors balance well to give reasonable reaction rates in the wide range of energy, which are shown in the inset of Figure 8 (the chained curve). Indeed, the rate thus evaluated consistently overestimates the true statistical values by the factor of only 1.4−1.8.

B. Distribution of Released Kinetic Energy. Figure 9 shows two normalized probability distributions and molecular dynamics counterparts for the distribution of released kinetic energy due to the monomer evaporation from Ar_8, where the energy was set to −12.0 and −8.0. The conditions of this calculation are similar to those specified in section IIA, except that 10 000 trajectories were used. The position of the dividing surface

estimated in the section IVB was also used as a place where $P(E,\epsilon_K)$ was estimated. Here again the agreements between the statistical and MD results are excellent. It thus turns out that the present nonempirical statistical approach predicts quite well such detailed dynamical information.

The kinetic energy distribution is one of the important physical observables that can be measured experimentally. Furthermore, it can be shown theoretically that one can argue a deep relationship between the distribution of released kinetic energy and the canonical temperature of clusters, which suggests how to determine experimentally the temperature of isolated clusters. This aspect will be reported elsewhere.[64]

VI. Concluding Remarks

We have studied the evaporation dynamics of an Ar_8-like Morse cluster on the basis of the phase-space-volume formula of Calvo and Labastie.[35] It has been numerically clarified that the evaporation couples very strongly with isomerization dynamics. In other words, the cluster keeps undergoing structural change frequently in the course of dissociation. Statistical rate theories that separate the vibration and rotation modes should miss this very important feature of dynamics. We therefore have studied a practical and nonempirical method to estimate the classical density of states and the flux for a highly nonrigid molecule having many flexible locally stable structures. There are two basic keys in our theoretical treatment: (i) In the calculation of the phase-space volume Ω and the flux W at the dividing surface, we did not separate vibrational and rotational modes by performing the relevant integrations in the full momentum space analytically under the conservation of linear and angular momenta. Thus the computation of Ω and W is essentially reduced to the calculation of the volume of configuration space $\Omega_Q(\epsilon)$ in the reactant area and in the dividing surface, respectively. (ii) We have devised a method to evaluate the absolute magnitude of $\Omega_Q(\epsilon)$ within the Monte Carlo technique by figuring out the integral measure.

The statistical treatment for the kinetic energy release, besides the total reaction rate, has been developed in the present paper. The rate constants and the kinetic energy release calculated by the statistical method have successfully reproduced the MD values quite accurately. We therefore think that the approach developed here is a useful step toward the study of multichannel chemical reactions of nonrigid molecules having many local potential basins. Although we have concentrated on the absolute rate constant and the kinetic energy release in this paper, there are still other interesting problems in the multichannel chemical reaction. The relationship between the angular momentum distribution and the shape of a cluster is among them.

Finally, we stress that the present method developed here is valid for the dimer evaporation too. Recently, much attention has been paid to the dimer evaporation for various clusters in the context of the branching ratio of the fragments in dissociation processes.[65−67] We will report the analysis of the dimer evaporation in a future publication.[27]

Acknowledgment. This work was supported in part by the Grant-in-aid for Basic Science and the 21st Century COE Program for Frontiers in Fundamental Chemistry from the Ministry of Education, Culture, Sports, Science, and Technology of Japan.

Appendix

Appendix A: Momentum Part Integrals. The phase-space volume (proportional to the Thomas−Fermi classical density of states), the flux (the sum of states at the dividing surface), and the (unnormalized) probability density of the kinetic energy release of our cluster are given in eqs 12, 13, and 26, respectively. For this paper to be self-contained as much as possible, we outline the phase-space volume formula by Calvo and Labastie[35] and our extension for the calculation of the flux and kinetic energy release.

1. Phase-Space Volume. We begin with the standard Hamiltonian

$$H = \sum_{i=1}^{N} \frac{p_i^2}{2m} + V(\{\mathbf{r}_i\}) \tag{A1}$$

where the masses of all the particles are taken to be equal (for more general cases, consult with ref 35). The phase-space volume under a conservation of the linear and angular momenta is represented as

$$\Omega(E,\mathbf{P},\mathbf{J}) = \int \prod_{i=1}^{N} \mathrm{d}\mathbf{r}_i\, \mathrm{d}\mathbf{p}_i\, \delta[H(\{\mathbf{r}_i\},\{\mathbf{p}_i\}) - E]\, \delta[\sum_{i=1}^{N} \mathbf{p}_i - \mathbf{P}]\, \delta[\sum_{i=1}^{N} \mathbf{j}_i - \mathbf{J}] \tag{A2}$$

We first define a $3N \times 6$ matrix $\mathbf{B}$ composed of 3×3 antisymmetric matrices $\mathbf{C}_i$ and the 3×3 identity tensor $\mathbf{1}(3)$:

$$\mathbf{B} = \begin{pmatrix} \mathbf{C}_1 & \mathbf{1}(3) \\ \vdots & \vdots \\ \mathbf{C}_N & \mathbf{1}(3) \end{pmatrix} \qquad \mathbf{C}_i = \begin{pmatrix} 0 & z_i & -y_i \\ -z_i & 0 & x_i \\ y_i & -x_i & 0 \end{pmatrix}$$

where $(x_i, y_i, z_i) = \mathbf{r}_i$ are the Cartesian coordinates of atom i. Then we have the following expression for the phase-space volume

$$\Omega(E,\mathbf{P},\mathbf{J}) = \int \mathrm{d}\tilde{\mathbf{R}}\, \Lambda(\tilde{\mathbf{R}},\mathbf{B},E,\mathbf{b}) \tag{A3}$$

$$\Lambda(\tilde{\mathbf{R}},\mathbf{B},E,\mathbf{b}) = \int \mathrm{d}\tilde{\mathbf{P}}\, \delta\left[\frac{\tilde{\mathbf{P}}^T\tilde{\mathbf{P}}}{2m} - \{E - V(\tilde{\mathbf{R}})\}\right] \delta[\mathbf{B}^{\mathrm{T}}\tilde{\mathbf{P}} - \mathbf{b}] \tag{A4}$$

where $\tilde{\mathbf{R}}$ and $\tilde{\mathbf{P}}$ are $3N$ vectors: $\tilde{\mathbf{P}} = (\mathbf{p}_1, ..., \mathbf{p}_N)^{\mathrm{T}}$ and $\tilde{\mathbf{R}} = (\mathbf{r}_1, ..., \mathbf{r}_N)^{\mathrm{T}}$. $\mathbf{b}$ is a 6-vector $\mathbf{b} = (\mathbf{J}, \mathbf{P})$. In the $3N$-dimensional momentum space, denoted as $\mathcal{L}$, for each configuration $\tilde{\mathbf{R}}$, the equation $\mathbf{B}^{\mathrm{T}}\tilde{\mathbf{P}} = 0$ defines a vector subspace $\mathcal{L}_1$ of dimension $3N - 6$, which in turn uniquely defines an orthogonal compliment $\mathcal{L}_2$. $\mathbf{U}$, U_1, and U_2 are now chosen as an orthonormal basis of $\mathcal{L}$, $\mathcal{L}_1$, and $\mathcal{L}_2$, respectively, such that

$$\mathbf{U} = (U_1, U_2) = (\mathbf{u}_{1,1}, \mathbf{u}_{1,2}, ..., \mathbf{u}_{1,3N-6}, \mathbf{u}_{2,1}, ..., \mathbf{u}_{2,6})$$

$\mathbf{U}$ has the following properties

$$\mathbf{U}^{\mathrm{T}}\mathbf{U} = \mathbf{1}(3N) \tag{A5}$$

$$\mathbf{B}^{\mathrm{T}}\mathbf{U} = (0|\mathbf{V}) \tag{A6}$$

where $\mathbf{1}(3N)$ is the $3N \times 3N$ identity tensor and $\mathbf{V}$ is a 6×6 matrix (should not be confused with the potential function).

With these new bases, the vector $\tilde{\mathbf{P}}$ can be expressed as $\mathbf{X} = \mathbf{U}^{\mathrm{T}}\tilde{\mathbf{P}} = (\mathbf{X}_1, \mathbf{X}_2)$ with $\mathbf{X}_1 \in \mathscr{L}_1$ and $\mathbf{X}_2 \in \mathscr{L}_2$, and Λ becomes

$$\Lambda = 2m\int \prod_{j=1}^{3N-6} \mathrm{d}X_{1,j} \prod_{k=1}^{6} \mathrm{d}X_{2,k}\, \delta[\mathbf{X}_1^{\mathrm{T}}\mathbf{X}_1 + \mathbf{X}_2^{\mathrm{T}}\mathbf{X}_2 - 2m\{E - V(\tilde{\mathbf{R}})\}]\, \delta[\mathbf{V}\mathbf{X}_2 - \mathbf{b}]|\det \mathbf{U}| \quad \text{(A7)}$$

We here change the variables from $\mathbf{X}_2$ to $\mathbf{X}_3 = \mathbf{V}\mathbf{X}_2$ and integrating on $\mathbf{X}_3$, and $\mathbf{X}_1$ leads to

$$\Lambda = 2m\frac{|\det \mathbf{U}|}{|\det \mathbf{V}|}\int \prod_{j=1}^{3N-6} \mathrm{d}X_{1,j}\, \delta[\mathbf{X}_1^{\mathrm{T}}\mathbf{X}_1 - \alpha] = \frac{(2m\pi)^{s/2}}{\Gamma\left(\frac{s}{2}\right)}\frac{|\det \mathbf{U}|}{|\det \mathbf{V}|}\left(E - V(\tilde{\mathbf{R}}) - \mathbf{b}^{\mathrm{T}}\frac{(\mathbf{V}\mathbf{V}^{\mathrm{T}})^{-1}}{2m}\mathbf{b}\right)^{(s-2)/2} \quad \text{(A8)}$$

where $\alpha = 2m\{E - \mathrm{V}(\tilde{\mathbf{R}})\} - \mathbf{b}^{\mathrm{T}}(\mathbf{V}\mathbf{V}^{\mathrm{T}})^{-1}\mathbf{b}$, $s = 3N - 6$, and $|\det \mathbf{U}|$ is unity from eq A5. Furthermore one can show

$$|\det \mathbf{V}| = m^{-3}M^{3/2}\sqrt{\det I_N} \quad \text{(A9)}$$

and

$$\mathbf{b}^{\mathrm{T}}\frac{(\mathbf{V}\mathbf{V}^{\mathrm{T}})^{-1}}{2m}\mathbf{b} = \frac{\mathbf{P}^2}{2M} + (\mathbf{J} - \mathbf{J}_{\mathrm{c}})^{\mathrm{T}}\frac{I_N^{-1}}{2}(\mathbf{J} - \mathbf{J}_{\mathrm{c}}) \quad \text{(A10)}$$

where $M = Nm$ is the total mass, I_N is the inertia tensor of the cluster with respect to the center-of-mass, and $\mathbf{J}_{\mathrm{c}}$ is the angular momentum of the center-of-mass. Substituting eqs A9 and A10 into eq A8, we have

$$\Lambda = \frac{(2\pi)^{s/2}m^{3N/2}}{\Gamma\left(\frac{s}{2}\right)M^{3/2}\sqrt{\det I_N}}\left(E - V(\tilde{\mathbf{R}}) - \frac{\mathbf{P}^2}{2M} - (\mathbf{J} - \mathbf{J}_{\mathrm{c}})^{\mathrm{T}}\frac{I_N^{-1}}{2}(\mathbf{J} - \mathbf{J}_{\mathrm{c}})\right)^{(s-2)/2} \quad \text{(A11)}$$

Bringing these back to the expression of the phase-space volume, we finally have

$$\Omega(E,\mathbf{P},\mathbf{J}) = \frac{(2\pi)^{s/2}m^{3N/2}}{\Gamma\left(\frac{s}{2}\right)M^{3/2}}\int \frac{\mathrm{d}\tilde{\mathbf{R}}}{\sqrt{\det I_N}}\left(E - V(\tilde{\mathbf{R}}) - \frac{\mathbf{P}^2}{2M} - (\mathbf{J} - \mathbf{J}_{\mathrm{c}})^{\mathrm{T}}\frac{I_N^{-1}}{2}(\mathbf{J} - \mathbf{J}_{\mathrm{c}})\right)^{(s-2)/2} \quad \text{(A12)}$$

By setting $m = 1$, one obtains eqs 12.

2. Flux. Next the flux integral in the case of the monomer evaporation is described. First, $\mathbf{u}_{1,1}$above should be chosen as

$$\mathbf{u}_{1,1} = \frac{1}{r_{\mathrm{re}}\sqrt{\frac{N}{N-1}}}\left(\mathbf{r}_{\mathrm{re}}, \frac{-1}{N-1}\mathbf{r}_{\mathrm{re}}, \ldots, \frac{-1}{N-1}\mathbf{r}_{\mathrm{re}}\right)^{\mathrm{T}} \quad \text{(A13)}$$

where $\mathbf{r}_{\mathrm{re}}$ is a vector connecting an evaporating atom and the daughter cluster, and r_{re} is its length. In this frame, the relation between r_{re} and $X_{1,1}$ is represented as

$$\dot{r}_{\mathrm{re}} = \frac{1}{\sqrt{mm_{\mathrm{r}}}}X_{1,1} \quad \text{(A14)}$$

where m_{r} is the reduced mass $m_{\mathrm{r}} = (N-1)m/N$. The flux is represented by the following expression in terms of the same quantities defined in the previous subsection

$$W(E,\mathbf{P},\mathbf{J}) = D_{\mathrm{g}}\int \mathrm{d}\tilde{\mathbf{R}}\, \delta[r_{\mathrm{re}} - r_{\mathrm{re}}^{\ddagger}]\, \lambda(\tilde{\mathbf{R}},\mathbf{B},E,\mathbf{b}) \quad \text{(A15)}$$

and

$$\lambda(\tilde{\mathbf{R}},\mathbf{B},E,\mathbf{b}) = 2m\int \prod_{j=1}^{3N-6} \mathrm{d}X_{1,j} \prod_{k=1}^{6} \mathrm{d}X_{2,k}\, \delta[\mathbf{X}_1^{\mathrm{T}}\mathbf{X}_1 + \mathbf{X}_2^{\mathrm{T}}\mathbf{X}_2 - 2m\{E - \mathrm{V}(\tilde{\mathbf{R}})\}]\, \delta[\mathbf{V}\mathbf{X}_2 - \mathbf{b}]\dot{r}_{\mathrm{re}} \quad \text{(A16)}$$

where the D_{g} is the degeneracy of the dissociative atom and the integration on $X_{1,1}$ is performed in the positive range only. We transform the variable $\mathbf{X}_2$ to $\mathbf{X}_3 = \mathbf{V}\mathbf{X}_2$ and integrate over $\mathbf{X}_3$, which leads to

$$\lambda = \frac{2}{|\det \mathbf{V}|}\sqrt{\frac{N}{N-1}}\int \prod_{j=1}^{3N-6} \mathrm{d}X_{1,j}\, \delta[\mathbf{X}_1^{\mathrm{T}}\mathbf{X}_1 - \alpha]X_{1,1} \quad \text{(A17)}$$

Integration over $\mathbf{X}_1$ and substituting eqs A9 and A10 into eq A17 give rise to

$$\lambda = \frac{2}{|\det \mathbf{V}|}\sqrt{\frac{N}{N-1}}\int \prod_{j=2}^{3N-6} \mathrm{d}X_{1,j} \int_0^{\infty} \mathrm{d}X_{1,1}\, \delta[{X_{1,1}}^2 + \sum_{j=2}^{3N-6} \mathrm{X}_{1,j}^2 - \alpha]X_{1,1} = \frac{(2\pi)^{(s-1)/2}m^{3N/2}}{\Gamma\left(\frac{s+1}{2}\right)M^{3/2}\sqrt{\det I_N}}\left(E - V(\mathbf{R}) - \frac{\mathbf{P}^2}{2M} - (\mathbf{J} - \mathbf{J}_{\mathrm{c}})^{\mathrm{T}}\frac{I_N^{-1}}{2}(\mathbf{J} - \mathbf{J}_{\mathrm{c}})\right)^{(s-1)/2} \quad \text{(A18)}$$

After all, the flux in the case of the monomer evaporation can be written as

$$W(E,\mathbf{P},\mathbf{J}) = \frac{D_{\mathrm{g}}(2\pi)^{(s-1)/2}m^{3N/2}}{\Gamma\left(\frac{s+1}{2}\right)M^{3/2}\sqrt{m_{\mathrm{r}}}}\int \mathrm{d}\tilde{\mathbf{R}}\frac{\delta[r_{\mathrm{re}} - r_{\mathrm{re}}^{\ddagger}]}{\sqrt{\det I_N}}\left(E - V(\tilde{\mathbf{R}}) - \frac{\mathbf{P}^2}{2M} - (\mathbf{J} - \mathbf{J}_{\mathrm{c}})^{\mathrm{T}}\frac{I_N^{-1}}{2}(\mathbf{J} - \mathbf{J}_{\mathrm{c}})\right)^{(s-1)/2} \quad \text{(A19)}$$

By setting $m = 1$, we obtain eq 13.

3. Kinetic Energy Release (KER). The integral crucial for the distribution of KER is discussed for the case of the vanishing total linear and angular momenta. Because of the rotational symmetry it is sufficient to carry out the integral with respect to a frame where the position vector of the dissociative atom (Nth atom) is represented as

$$\mathbf{r}_N = (x_N, y_N, z_N)^{\mathrm{T}} = \left(\frac{N-1}{N}r_{\mathrm{re}}^{\ddagger}, 0, 0\right)^{\mathrm{T}} \quad \text{(A20)}$$

In this frame the (unnormalized) probability density of the KER is written as

$$P_u(E,\epsilon_K) = \int\prod_{i=1}^{N-1} d\mathbf{r}_i\, d\mathbf{p}_i \int d\mathbf{p}_N\, \delta\left[\sum_{i=1}^{N-1}\mathbf{r}_i + \left(\frac{N-1}{N}r_{re}^{\ddagger}, 0, 0\right)^T\right] \times \delta[\sum_{i=1}^{N-1}\mathbf{p}_i + \mathbf{p}_N]\, \delta[\sum_{i=1}^{N-1}\mathbf{j}_i + \mathbf{j}_N]\dot{r}_{re}\, \delta[E - H(\{\mathbf{r}_i\},\{\mathbf{p}_i\})] \times \delta\left[\epsilon_K - \left(\frac{1}{2}m_r\dot{r}_{re}^{\ 2} + \frac{1}{2}\mathbf{L}^T I_L^{\ -1}\mathbf{L} + \frac{1}{2}\mathbf{J}_{N-1}I_{N-1}^{\ -1}\mathbf{J}_{N-1}\right)\right] \quad (A21)$$

and both the angular momentum of the daughter cluster $\mathbf{J}_{N-1}$ and the orbital angular momentum of the two fragments $\mathbf{L}$ depend on the momentum of the Nth atom, $\mathbf{p}_N$ in such a way that

$$\mathbf{J}_{N-1} = -\frac{N}{N-1}\mathbf{j}_N \qquad \mathbf{L} = \frac{N}{N-1}\mathbf{j}_N$$
$$\mathbf{j}_N = (0, -x_N p_{Nz}, x_N p_{Ny})^T \quad (A22)$$

Furthermore, the kinetic energy release is also written as a function of the $\mathbf{p}_N$, that is

$$\frac{1}{2}m_r\dot{r}_{re}^{\ 2} + \frac{1}{2}\mathbf{L}^T I_L^{\ -1}\mathbf{L} + \frac{1}{2}\mathbf{J}_{N-1}I_{N-1}^{\ -1}\mathbf{J}_{N-1} = \frac{(\sum_{i=1}^{N-1}\mathbf{p}_i)^2}{2M_{N-1}} + \frac{\mathbf{p}_N^{\ 2}}{2m} + \frac{1}{2}\left(\frac{N}{N-1}\right)^2 \mathbf{j}_N^T I_{N-1}^{\ -1}\mathbf{j}_N = \frac{\mathbf{p}_N^{\ 2}}{2m_r} + \frac{r_{re}^{\ddagger 2}}{2}\tilde{\mathbf{p}}_N^T\tilde{I}_{N-1}\tilde{\mathbf{p}}_N \quad (A23)$$

where $\dot{r}_{re} = p_{Nx}/m_r$, M_{N-1} is the mass of the daughter cluster, $\tilde{\mathbf{p}}_N$ is a 2-vector $\tilde{\mathbf{p}}_N = (p_{Ny}, p_{Nz})^T$, and $\tilde{I}_{N-1}$ is a 2×2 matrix

$$\tilde{I}_{N-1} = \begin{pmatrix} (I_{N-1}^{\ -1})_{zz} & -(I_{N-1}^{\ -1})_{zy} \\ -(I_{N-1}^{\ -1})_{zy} & (I_{N-1}^{\ -1})_{yy} \end{pmatrix} \quad (A24)$$

Substituting eq A23 into eq A21 and integrating out the kinetic part of the daughter cluster ($\prod_{i=1}^{N-1} d\mathbf{p}_i$) lead to

$$P_u(E,\epsilon_K) = \int\frac{\prod_{i=1}^{N-1} d\mathbf{r}_i}{\sqrt{\det I_{N-1}}}\delta\left[\sum_{i=1}^{N-1}\mathbf{r}_i + \left(\frac{N-1}{N}r_{re}^{\ddagger},0,0\right)^T\right] \times \frac{(2\pi)^{\tilde{s}/2}m^{3(N-1)/2}}{\Gamma(\tilde{s}/2)M_{N-1}^{\ 3/2}}(E - V(\{\mathbf{r}_i\}) - \epsilon_K)^{(\tilde{s}-2)/2} \times \int d\mathbf{p}_N \frac{p_{Nx}}{m_r}\delta\left[\epsilon_K - \left(\frac{\mathbf{p}_N^{\ 2}}{2m_r} + \frac{r_{re}^{\ddagger 2}}{2}\tilde{\mathbf{p}}_N^T\tilde{I}_{N-1}\tilde{\mathbf{p}}_N\right)\right] \quad (A25)$$

where $\tilde{s} = 3(N-1) - 6$. Then, we define λ_1, λ_2, and $\tilde{U}_{N-1}$ as eigenvalues of the $\tilde{I}_{N-1}$ and a matrix to diagonalize $\tilde{I}_{N-1}$. $\tilde{U}_{N-1}$ defines a coordinate transformation from (p_{Ny}, p_{Nz}) to (ξ_1, ξ_2), which is applied to eq A25 as

$$P_u(E,\epsilon_K) = \int\frac{\prod_{i=1}^{N-1} d\mathbf{r}_i}{\sqrt{\det I_{N-1}}}\delta\left[\sum_{i=1}^{N-1}\mathbf{r}_i + \left(\frac{N-1}{N}r_{re}^{\ddagger},0,0\right)^T\right] \times \frac{(2\pi)^{\tilde{s}/2}m^{3(N-1)/2}}{\Gamma(\tilde{s}/2)M_{N-1}^{\ 3/2}}(E - V(\{\mathbf{r}_i\}) - \epsilon_K)^{(\tilde{s}-2)/2}\int dp_{Nx}\int d\xi_1 \int d\xi_2 \frac{p_{Nx}}{m_r}\delta\left[\epsilon_K - \left\{\frac{\mathbf{p}_N^{\ 2}}{2m_r} + \frac{r_{re}^{\ddagger 2}}{2}(\lambda_1\xi_1^{\ 2} + \lambda_2\xi_2^{\ 2})\right\}\right]$$
$$= \int\frac{\prod_{i=1}^{N-1} d\mathbf{r}_i}{\sqrt{\det I_{N-1}}}\delta\left[\sum_{i=1}^{N-1}\mathbf{r}_i + \left(\frac{N-1}{N}r_{re}^{\ddagger},0,0\right)^T\right] \times \frac{(2\pi)^{\tilde{s}/2}m^{3(N-1)/2}}{\Gamma(\tilde{s}/2)M_{N-1}^{\ 3/2}}(E - V(\{\mathbf{r}_i\}) - \epsilon_K)^{(\tilde{s}-2)/2}\frac{\pi\epsilon_K}{\sqrt{\Lambda_1\Lambda_2}} \quad (A26)$$

where

$$\Lambda_l = \frac{1}{2m_r} + \frac{r_{re}^{\ddagger 2}}{2}\lambda_l \qquad \text{for} \qquad l = 1, 2$$

The relation between the inertia tensor of the parent cluster and the daughter cluster can be proved as

$$\det I_N = (2m_r)^2\Lambda_1\Lambda_2 \det I_{N-1} \quad (A27)$$

Substituting eq A27 into eq A26 leads to the final form

$$P_u(E,\epsilon_K) = \frac{m^{3N/2}}{m_r^{\ 1/2}M^{3/2}}\int\frac{\prod_{i=1}^{N-1} d\mathbf{r}_i}{\sqrt{\det I_N}} \times \delta\left[\sum_{i=1}^{N-1}\mathbf{r}_i + \left(\frac{N-1}{N}r_{re}^{\ddagger},0,0\right)^T\right]\frac{(2\pi)^{\tilde{s}/2}}{\Gamma(\tilde{s}/2)} \times (E - V(\{\mathbf{r}_i\}) - \epsilon_K)^{(\tilde{s}-2)/2}2\pi\epsilon_K \quad (A28)$$

This can be written in the convolution form as

$$P_u(E,\epsilon_K) = \int_0^{E-\epsilon_K} d\epsilon\ \Omega_Q^{\ddagger}(\epsilon)\ \Omega_{P,N-1}(E-\epsilon-\epsilon_K)\ W_r(\epsilon_K) \quad (A29)$$

$$\Omega_Q^{\ddagger}(\epsilon) = \frac{m^{3N/2}}{M^{3/2}m_r^{\ 1/2}}\int\prod_{i=1}^{N-1} d\mathbf{r}_i \frac{\delta[\epsilon - V(\{\mathbf{r}_i\})]}{\sqrt{\det I_N}} \times \delta\left[\sum_{i=1}^{N-1}\mathbf{r}_i + \left(\frac{N-1}{N}r_{re}^{\ddagger},0,0\right)^T\right] \quad (A30)$$

$$\Omega_{P,N-1}(K) = \frac{(2\pi)^{\tilde{s}/2}}{\Gamma(\tilde{s}/2)}K^{(\tilde{s}-2)/2} \quad (A31)$$

$$W_r(\epsilon_K) = 2\pi\epsilon_K \quad (A32)$$

The configuration-space density of states in the dividing surface, which is written as eq A30 in the specific frame mentioned

above, can be written as eq 17 in the general Cartesian frame that sets the origin to the center-of-mass of the parent cluster. (Note that the masses of the particles were set to unity and the rotational and permutation symmetries of the particles were taken account in eq 17.)

References and Notes

(1) Jellinek, J.; Beck, L. T.; Berry, S. R. *J. Chem. Phys.* **1986**, *84*, 2783.
(2) Amar, G. F.; Berry, S. R. *J. Chem. Phys.* **1986**, *85*, 5943.
(3) Berry, S. R.; Beck, L. T.; Davis, L. H.; Jellinek, J. *Adv. Chem. Phys.* **1988**, *70*, 75.
(4) Labastie, P.; Whetten, L. R. *Phys. Rev. Lett* **1990**, *65*, 1567.
(5) Seko, C.; Takatsuka, K. *J. Chem. Phys.* **1996**, *104*, 8613.
(6) Seko, C.; Takatsuka, K. *J. Chem. Phys.* **1998**, *108*, 4924.
(7) Seko, C.; Takatsuka, K. *J. Chem. Phys.* **1998**, *109*, 4768.
(8) Takatsuka, K.; Seko, C. *J. Chem. Phys.* **1996**, *105*, 10356.
(9) Takatsuka, K.; Seko, C. *J. Chem. Phys.* **1999**, *110*, 3263.
(10) Yanao, T.; Takatsuka, K. *Chem. Phys. Lett.* **1999**, *313*, 633.
(11) Takatsuka, K.; Yanao, T. *J. Chem. Phys.* **2000**, *113*, 2552.
(12) Takatsuka, K. *Adv. Chem. Phys. Part B* **2005**, *130*, 25.
(13) Yanao, T.; Takatsuka, K. *Phys. Rev. A* **2003**, *68*, 03714.
(14) Yanao, T.; Takatsuka, K. *J. Chem. Phys.* **2004**, *120*, 8924.
(15) Yanao, T.; Takatsuka, K. *Adv. Chem. Phys. Part B* **2005**, *130*, 87.
(16) Teramoto, H.; Takatsuka, K. *J. Chem. Phys.* **2005**, *122*, 074101.
(17) Inoue-Ushiyama, A.; Takatsuka, K. *Phys. Rev. E* **2001**, *64*, 056223.
(18) Amitrano, C.; Berry, S. R. *Phys. Rev. Lett* **1992**, *68*, 729.
(19) Amitrano, C.; Berry, S. R. *Phys. Rev. E* **1993**, *47*, 3158.
(20) Hinde, J. R.; Berry, S. R.; Wales, J. D. *J. Chem. Phys.* **1992**, *96*, 1376.
(21) Hinde, J. R.; Berry, S. R. *J. Chem. Phys.* **1993**, *99*, 2942.
(22) Komatsuzaki, T.; Berry, S. R. *J. Chem. Phys.* **1999**, *110*, 9160.
(23) Komatsuzaki, T.; Berry, S. R. *J. Chem. Phys.* **2001**, *115*, 4105.
(24) Berry, S. R. *Chem. Rev.* **1993**, *93*, 2379.
(25) Braief, A. P.; Berry, S. R. *J. Chem. Phys.* **1990**, *93*, 8745.
(26) Miller, A. M.; Doye, K. P. J.; Wales, J. D. *J. Chem. Phys.* **1999**, *110*, 328.
(27) Fujii, M.; Takatsuka, K. To be published.
(28) Steinfeld, I. S.; Francisco, J. S.; Hase W. L. *Chemical Kinetics and Dynamics*; Prentice Hall: Englewood Cliffs, NJ, 2004.
(29) Wigner, P. E. *J. Chem. Phys.* **1937**, *5*, 720.
(30) Keck, C. J. *J. Chem. Phys.* **1960**, *32*, 1035.
(31) Light, C. J. *J. Chem. Phys.* **1964**, *40*, 3221.
(32) Weerasinghe, S.; Amar, G. F. *J. Chem. Phys.* **1993**, *98*, 328.
(33) Parneix, P.; Bréchignac, Ph.; Amar, G. F. *J. Chem. Phys.* **1996**, *104*, 983.
(34) Parneix, P.; Amar, G. F.; Bréchignac, Ph. *Chem. Phys.* **1998**, *239*, 121.
(35) Calvo, F.; Labastie, P. *Eur. Phys. J. D* **1998**, *3*, 229.
(36) Calvo, F. *J. Phys. Chem. B* **2001**, *105*, 2183.
(37) Calvo, F.; Parneix, P. *J. Chem. Phys.* **2003**, *119*, 256.
(38) Calvo, F.; Parneix, P. *J. Chem. Phys.* **2003**, *119*, 9469.
(39) Parneix, P.; Calvo, F. *J. Chem. Phys.* **2004**, *120*, 2780.
(40) Chesnavich, J. W.; Bowers, T. M. *J. Chem. Phys.* **1977**, *66*, 2306.
(41) Smith, C. S. *J. Chem. Phys.* **1991**, *95*, 3403.
(42) Smith, C. S. *J. Chem. Phys.* **1992**, *97*, 2406.
(43) Reinhardt, P. W. *J. Mol. Struct.* **1990**, *223*, 157.
(44) Watanabe, M.; Reinhardt, P. W. *Phys. Rev. Lett.* **1990**, *65*, 3301.
(45) Yoshida, H. *Phys. Lett. A* **1990**, *150*, 262.
(46) Stillinger, H. F.; Weber, A. T. *Phys. Rev. A* **1982**, *25*, 978.
(47) Fukui, K. *J. Phys. Chem.* **1970**, *74*, 4161.
(48) For a recent review, see: Yang, X.; Liu, K. *Modern Trends in Chemical Reaction Dynamics*; World Scientific: Singapore, 2004; Chapter 7.
(49) Troe, J. *J. Chem. Phys.* **1977**, *66*, 4758.
(50) Hertz, P. *Ann. Phys.* **1910**, *33*, 537.
(51) Note that ergodicity is an independent notion from that of chaos. For instance, multiply periodic motion is ergodic on a torus but not chaotic.
(52) Rough, H. H. *Phys. Rev. E* **2001**, *64*, 055101.
(53) Adib, B. A. *Phys. Rev. E* **2002**, *66*, 047101.
(54) Because the Thomas−Fermi density of states is $(2\pi\hbar)^{-n}\Omega(E,\mathbf{P},\mathbf{J})$, they are quite often identified vaguely as a same quantity. We too sometimes call $\Omega(E,\mathbf{P},\mathbf{J})$ simply the density of states without notice.
(55) Dumont, S. R. *J. Chem. Phys.* **1991**, *95*, 9172.
(56) Nyman, G.; Nordholm, S.; Schranz, W. H. *J. Chem. Phys.* **1990**, *93*, 6767.
(57) Wang, F.; Landau, P. D. *Phys. Rev. Lett.* **2001**, *86*, 2050.
(58) Horiuti, J. *Bull. Chem. Soc. Jpn.* **1938**, *13*, 210.
(59) (a) Truhlar, G. D.; Garrett, C. B. *Acc. Chem. Res.* **1980**, *13*, 440. (b) Dykstra, E. C.; Frenking, G.; Kim, K.; Scuseria, G. *Theory and Applications of Computational Chemistry*; Elsevier: Amsterdam, 2005; p 67.
(60) Uzer, T.; Jaffé, C.; Palacian, J.; Yanguas, P.; Wiggins, S. *Nonlinearity* **2002**, *15*, 957.
(61) Komatsuzaki, T.;Berry, S. R. *Adv. Chem. Phys. Pt. A* **2005**, *130*, 143.
(62) Jaffé, C.; Kawai, S.; Alacián, J.; Yanguas, P.; Uzer, T. *Adv. Chem. Phys. Pt. A* **2005**, *130*, 171.
(63) Hase, L. W. *Acc. Chem. Res.* **1983**, *16*, 258.
(64) Fujii, M.; Takatsuka, K. To be published.
(65) Rytkönen, A.; Manninen, M. *J. Chem. Phys.* **2000**, *113*, 4647.
(66) Napari, I.; Vehkamäki, H. *J. Chem. Phys.* **2004**, *121*, 819.
(67) Díaz-Tendero, S.; Hervieux, -A. P.; Alcamí, M.; Martín, F. *Phys. Rev. A* **2005**, *71*, 033202.